

Stable single-layers of calcium halides (CaX_2 , X = F, Cl, Br, I)

Cite as: J. Chem. Phys. **152**, 164116 (2020); <https://doi.org/10.1063/5.0006011>

Submitted: 27 February 2020 • Accepted: 01 April 2020 • Published Online: 29 April 2020

 M. Baskurt,  M. Yagmurcukardes,  F. M. Peeters, et al.

COLLECTIONS

Paper published as part of the special topic on [2D Materials](#)



View Online



Export Citation



CrossMark

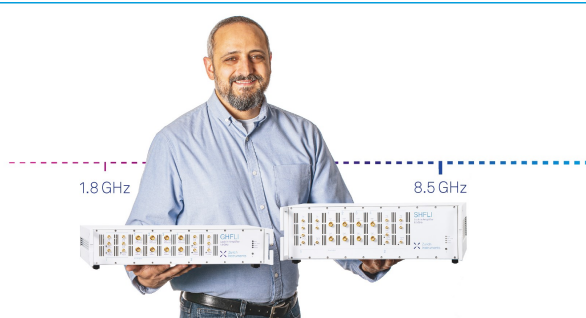
ARTICLES YOU MAY BE INTERESTED IN

[Quantum properties and applications of 2D Janus crystals and their superlattices](#)
Applied Physics Reviews **7**, 011311 (2020); <https://doi.org/10.1063/1.5135306>

[Hybrid functionals based on a screened Coulomb potential](#)
The Journal of Chemical Physics **118**, 8207 (2003); <https://doi.org/10.1063/1.1564060>


[A consistent and accurate ab initio parametrization of density functional dispersion correction \(DFT-D\) for the 94 elements H-Pu](#)
The Journal of Chemical Physics **132**, 154104 (2010); <https://doi.org/10.1063/1.3382344>





Trailblazers. New

Meet the Lock-in Amplifiers that measure microwaves.

 Zurich Instruments [Find out more](#)

Stable single-layers of calcium halides (CaX₂, X = F, Cl, Br, I)

Cite as: J. Chem. Phys. 152, 164116 (2020); doi: 10.1063/5.0006011

Submitted: 27 February 2020 • Accepted: 1 April 2020 •

Published Online: 29 April 2020



View Online



Export Citation



CrossMark

M. Baskurt,¹  M. Yagmurcukardes,^{2,a)}  F. M. Peeters,²  and H. Sahin¹ 

AFFILIATIONS

¹Department of Photonics, Izmir Institute of Technology, Izmir, Turkey

²Department of Physics, University of Antwerp, Groenenborgerlaan 171, B-2020 Antwerp, Belgium

Note: This paper is part of the JCP Special Topic on 2D Materials.

a) Author to whom correspondence should be addressed: mehmetyagmurcukardes.edu@gmail.com

ABSTRACT

By means of density functional theory based first-principles calculations, the structural, vibrational, and electronic properties of 1H- and 1T-phases of single-layer CaX₂ (X = F, Cl, Br, or I) structures are investigated. Our results reveal that both the 1H- and 1T-phases are dynamically stable in terms of their phonon band dispersions with the latter being the energetically favorable phase for all single-layers. In both phases of single-layer CaX₂ structures, significant phonon softening occurs as the atomic radius increases. In addition, each structural phase exhibits distinctive Raman active modes that enable one to characterize either the phase or the structure via Raman spectroscopy. The electronic band dispersions of single-layer CaX₂ structures reveal that all structures are indirect bandgap insulators with a decrease in bandgaps from fluorite to iodide crystals. Furthermore, the calculated linear elastic constants, in-plane stiffness, and Poisson ratio indicate the ultra-soft nature of CaX₂ single-layers, which is quite important for their nanoelastic applications. Overall, our study reveals that with their dynamically stable 1T- and 1H-phases, single-layers of CaX₂ crystals can be alternative ultra-thin insulators.

Published under license by AIP Publishing. <https://doi.org/10.1063/5.0006011>

I. INTRODUCTION

The discovery of graphene sparked great interest in two-dimensional (2D) ultra-thin materials.^{1,2} Following graphene, many novel 2D materials such as transition metal dichalcogenes (TMDs),^{3–12} Xenes (X = Si, Ge, Sn, and Pb),^{13–20} magnetic monolayers,^{21–26} and hexagonal boron nitride (*h*-BN)²⁷ have been extensively studied as important members of the 2D family and have been utilized in various nanoscale device applications. Among 2D materials, *h*-BN is a well-known insulator that has been widely used as a separator in van der Waals heterostructures.²⁸ As a heterojunction diode was fabricated using *h*-BN as the insulating layer, its performance was reported to be comparable to the classical *p*-*n* junction diodes.²⁹ In addition, the use of *h*-BN in the development of atomically thin integrated circuits has brought a new approach for novel low dimensional electronics.³⁰ Moreover, using *h*-BN as an encapsulating agent was reported to efficiently enhance the stability of TMDs.³¹

Calcium halides are inorganic materials possessing great potential in various applications. Among calcium halides, CaF₂ is known

as the fundamental source for the synthesis of hydrofluoric acid.³² CaF₂ has been widely used in dental practice in order to cover dental cavities^{33–37} and has also been used in high-power diode pumps and ceramic lasers.^{38–42} On the other hand, due to its insulating property, CaF₂ has been an appealing material in micro- and nano-electronics. In our previous study, a single-layer CaF₂ in the 1T structure was investigated and substantial properties were presented and compared to the well-known single-layer insulator *h*-BN.⁴³ CaCl₂ is another important member of Ca-halides, which has been extensively used in electrolyte solutions.⁴⁴ In addition, CaCl₂ was reported to increase the capture performance of CO₂, making it an important candidate for reducing the energy consumption and increasing the capture capacity.^{45,46} Moreover, CaCl₂ plays an important role in extending the shelf life of fruits and vegetables, making it suitable for applications in agricultural and food chemistry.^{47–49} Furthermore, mixing of CaCl₂ with another calcium halide, CaBr₂, was shown to be a good process for ammonia storage.^{50,51} CaBr₂ was used in alteration of the vapor-liquid equilibrium of the acetone and methanol system, resulting in elimination of the azeotropic point of the

system completely and granting it for obtaining ideal gas behavior.⁵² Moreover, CaBr_2 was reported as an instant and renewable brominating agent for substituted aromatics, which increases the demand in industrial and pharmaceutical fields.⁵³ Likewise the other calcium halide, CaI_2 , was shown to have applications in numerous areas such as to be an excellent catalytic agent for the synthesis of carbonates from epoxides.^{54–56} Additionally, laser excitation of CaI_2 in ethanol solution revealed the formation of cluster ions in mass spectrometric analysis. Due to the layered structure, CaI_2 is reported as a material that can be exfoliated into a single-layer with a relatively low cleavage energy.^{57,58} Apparently, bulk calcium halides have various important application fields. However, investigation of ultra-thin structures of calcium halides is quite important for their nanodevice applications, which have been mainly ignored in previous studies.

In this study, the structural, vibrational, electronic, and mechanical properties of single-layer calcium halide (CaX_2) structures are investigated using first-principles calculations. CaX_2 s in 1T and 1H structures are found to be dynamically stable. Raman active modes are predicted by the characteristics of the vibrational modes in phonon calculations. Raman spectra are shown to exhibit rich information for the characterization of structural phases of a single-layer CaX_2 and even for the distinguishing of the structures having the same phase. In addition, the insulating behavior of all single-layer CaX_2 is shown to make them alternative materials to the well-known ultra-thin insulator *h*-BN. Moreover, the trends between calcium halide structures and their charge transfer, in-plane stiffness, cohesive energy, and work function are discussed.

II. COMPUTATIONAL METHODOLOGY

First-principles calculations within density functional theory (DFT) were performed to investigate the structural, vibrational, and electronic properties of single-layer CaX_2 s in 1T and 1H structures using the Vienna *ab initio* Simulation Package (VASP).^{59,60} Plane-wave projector-augmented wave (PAW)⁶¹ potentials were used in the calculations. For the exchange–correlation functional, the generalized gradient approximation (GGA) form of Perdew–Burke–Ernzerhof (PBE)⁶² was used. The DFT-D2 method of Grimme was employed as the van der Waals corrections.⁶³ The Heyd–Scuseria–Ernzerhof (HSE06) functional was employed in order to increase the accuracy of electronic structure calculations.⁶⁴ The Bader technique was used to determine the charge transfer in the system.⁶⁵

The kinetic energy cutoff of the plane-wave basis set was taken to be 500 eV, and the Gaussian broadening width was taken to be 0.05 eV for the structural optimizations and the electronic properties. The convergence criteria between consequent steps were set to be 10^{-5} eV. In order to prevent any interactions in the non-periodic direction, a 15 Å of vacuum spacing was inserted between the adjacent layers. A Γ centered *k*-point mesh was taken to be $7 \times 7 \times 1$ for structural optimizations. A $13 \times 13 \times 1$ *k*-mesh was taken for calculation of charge density eigenvalues, which were employed in calculating the electronic band structures. Geometric relaxation of atoms within the primitive cells was allowed until pressures became less than 1 kB in all directions. Additionally, a small displacement method implemented within the PHON code was used to calculate the phonon band dispersions.⁶⁶

III. RESULTS AND DISCUSSION

A. Structural, vibrational, and elastic properties

Single-layer CaX_2 structures can be formed either in 1H or 1T phases by truncation from their bulk or by growing in a different orientation on a substance. In this study, the 1H and 1T phases of CaX_2 single-layers are investigated, and their dynamical stabilities are examined via phonon band dispersions through the whole Brillouin zone (BZ). The 1T-phase structure [see Fig. 1(a)] is composed of a Ca layer sandwiched between two halogen atom layers leading to the $P\bar{3}m2$ space-group-symmetry. On the other hand, the 1H-phase [see Fig. 1(b)] in which a Ca atom is sandwiched between two halogen atom layers, which are separated symmetrically with respect to the Ca layer, exhibits $P6/m\bar{2}$ space-group-symmetry. For all CaX_2 structures, the 1T-phase is found to be energetically more favorable as compared to the 1H-phase. The total energy differences per primitive unit cell are calculated to be 0.73 eV, 0.43 eV, 0.35 eV, and 0.28 eV for structures of F, Cl, Br, and I, respectively. As listed in Table I, the optimized in-plane lattice parameters of 1T- CaX_2 vary between 3.58 Å and 4.47 Å as the halogen atom changes from F to I. On the other hand, those for the 1H-phase are quite smaller from those of the 1T-phase and are found to vary between 3.40 Å and 4.32 Å. Notably, as the atomic radius of the halogen atom increases, the corresponding in-plane lattice parameters increase in both phases accordingly. The Bader charge analysis reveals that in 1T- CaX_2 structures, each Ca donates its 1.6 *e* to halogens. Similarly, in 1H structures, each Ca atom donates its 1.5 *e* to halogen atoms in 1H- CaX_2 . Moreover, as listed in Table I, the cohesive energies per atom decrease as the atomic radius increases in both phases of CaX_2 structures. In addition, cohesive energies of the bulk CaX_2 structures are calculated. Bulk CaF_2 , which possesses $Fm\bar{3}m$ space-group-symmetry, has a cohesive energy of 5.62 eV/atom. Bulk CaCl_2 and CaBr_2 structures with $Pn\bar{m}$ and $P4_2/m\bar{m}$ space-group-symmetries have cohesive energies per atom of 4.20 eV/atom and 3.79 eV/atom, respectively. Bulk CaI_2 with a layered structure ($P\bar{3}m1$ space-group) has a cohesive energy of 3.42 eV/atom.

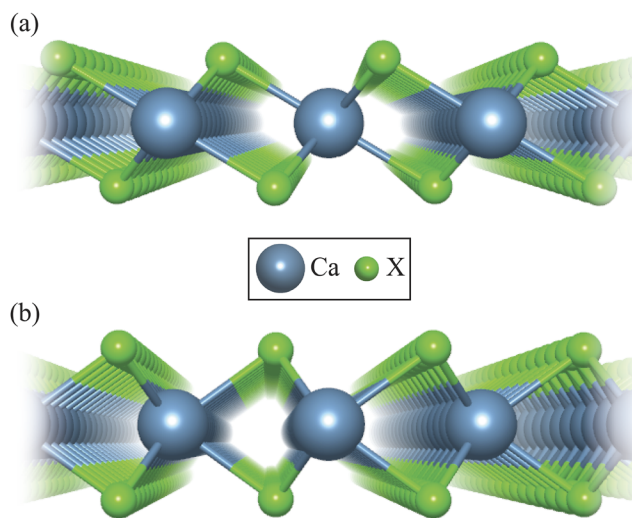


FIG. 1. Crystal structures of (a) 1T- CaX_2 and (b) 1H- CaX_2 ($X = \text{F}, \text{Cl}, \text{Br}, \text{and I}$).

TABLE I. Calculated parameters for single-layer CaX_2 s: optimized in-plane lattice constants ($a = b$), bond length between a Ca atom and the halogen ($d_{\text{Ca-X}}$), distance between X atoms ($d_{\text{X-X}}$), the X–Ca–X bond angle (θ), donated electron by per Ca (ρ_{Ca}), cohesive energy per atom in the unit cell (E_c), work function (Φ), energy bandgaps calculated within GGA ($E_{\text{gap}}^{\text{GGA}}$) and within HSE06 on top of GGA ($E_{\text{gap}}^{\text{HSE06}}$), in plane stiffness (C), Poisson ratio (ν), and the frequencies of the Raman active modes.

	Phase	a (Å)	$d_{\text{Ca-X}}$ (Å)	$d_{\text{X-X}}$ (Å)	θ (°)	ρ_{Ca} (e^-)	E_c (eV/atom)	Φ (eV)	$E_{\text{gap}}^{\text{GGA}}$ (eV)	$E_{\text{gap}}^{\text{HSE06}}$ (eV)	C (N/m)	ν	R-active modes (cm^{-1})
CaF ₂	1T	3.58	2.29	2.84	76.88	1.6	5.42	8.67	7.17	9.49	44	0.24	281, 299
	1H	3.40	2.31	2.43	63.56	1.6	5.17	10.13	6.34	8.73	38	0.49	134, 268, 414
CaCl ₂	1T	4.10	2.76	3.70	84.09	1.6	4.17	7.98	5.79	7.57	22	0.21	149, 183
	1H	3.90	2.78	3.27	72.03	1.5	4.03	8.10	4.82	6.46	24	0.42	86, 180, 233
CaBr ₂	1T	4.24	2.92	4.02	86.92	1.5	3.77	7.39	4.95	6.55	18	0.22	87, 114
	1H	4.06	2.95	3.58	74.67	1.5	3.65	7.46	4.19	5.65	22	0.40	52, 143, 147
CaI ₂	1T	4.47	3.15	4.45	89.71	1.5	3.36	6.46	3.79	5.11	16	0.24	62, 84
	1H	4.32	3.19	3.97	77.07	1.5	3.26	6.42	3.19	4.38	21	0.37	40, 105, 132

The dynamical stabilities of the 1T and 1H phases are also verified by calculating their phonon band dispersions through the whole BZ. As presented in Fig. 2, both 1T and 1H phases of the single-layer CaX_2 are free from imaginary frequencies in the whole BZ, indicating their dynamical stability. In both phases, there are six optical phonon branches whose vibrational characteristics are shown on the right panel of the phonon band dispersions in Fig. 2. As a result of the in-plane isotropy of the structures, there exist two doubly degenerate in-plane and two non-degenerate out-of-plane phonon modes in both phases of single-layer CaX_2 structures. 1T- CaX_2 crystals possess C_{3v} symmetry, and the corresponding Raman active modes are denoted as A_{1g} and E_g . In both phonon modes, the Ca atom has no contribution to the vibration, while the halogen atoms vibrate out-of-phase against each other in the out-of-plane and in-plane

directions, respectively. In all single-layer 1T- CaX_2 , the frequency of A_{1g} is calculated to be higher than that of E_g , and both phonon modes display phonon softening as the atomic mass of halogen increases. For the 1H- CaX_2 structures, there are two doubly degenerate in-plane (E' and E'') and a non-degenerate out-of-plane (A_1) Raman active modes. The E'' mode is attributed to the in-plane vibration of halogens against each other, and it has the lowest frequency in each single-layer structure. In E' phonon mode, the Ca atom and the two halogen atoms vibrate out-of-phase in lateral directions. The other Raman active mode, A_1 , is originated from the out-of-plane vibration of two halogen atoms against each other. In 1H-phases of CaF_2 and CaCl_2 , A_1 has a higher frequency than the E' mode, indicating that the vertical component of the force constant between Ca–F and Ca–Cl is larger than the lateral component.

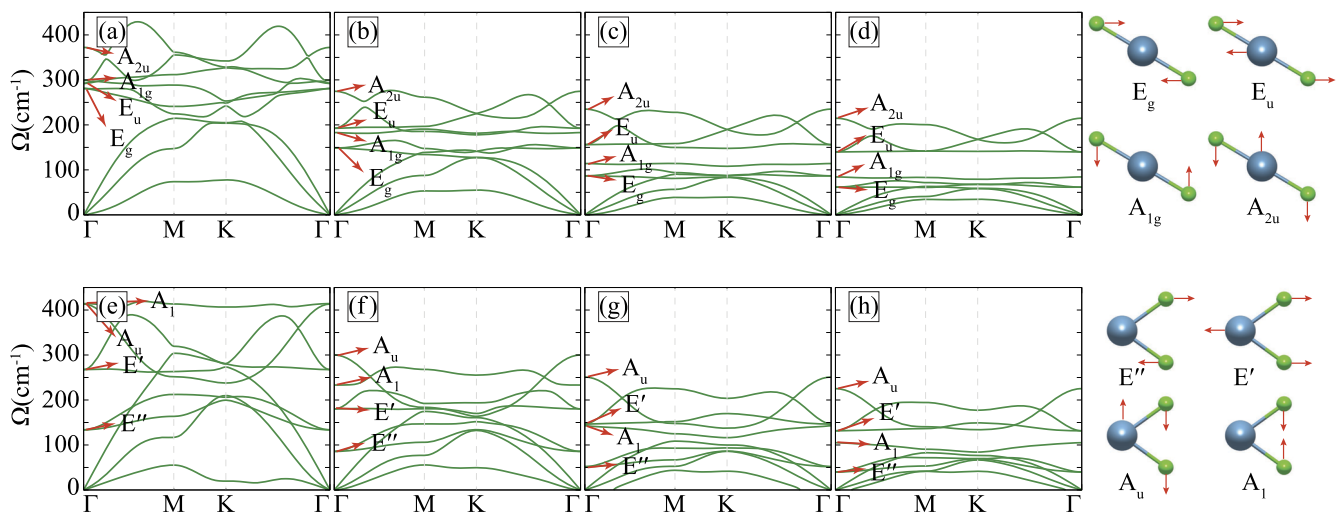


FIG. 2. Phonon dispersions of (a) 1T- CaF_2 , (b) 1T- CaCl_2 , (c) 1T- CaBr_2 , (d) 1T- CaI_2 , (e) 1H- CaF_2 , (f) 1H- CaCl_2 , (g) 1H- CaBr_2 , and (h) 1H- CaI_2 . The corresponding vibrational modes are presented in the inset.

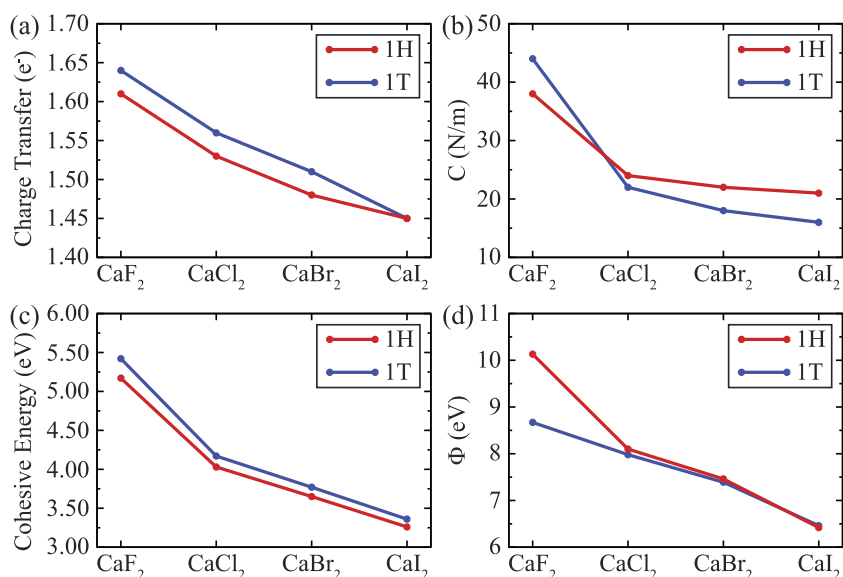


FIG. 3. Graph of (a) CaX_2 s vs charge transfer, (b) CaX_2 vs in-plane stiffness, (c) CaX_2 vs cohesive energy, and (d) CaX_2 vs work function.

However, as the atomic mass increases, the lateral component of the force constant between Ca-Br and Ca-I becomes dominant to that of the vertical component. Therefore, in CaBr_2 and CaI_2 , the E' phonon mode has a higher frequency than that of the A_1 mode.

The in-plane stiffness, C , which is a measure of the rigidity of a material, and the Poisson ratio, ν , which is the ratio of the transverse contraction strain to the longitudinal extension, describe the linear elastic properties of 2D materials. In order to determine the

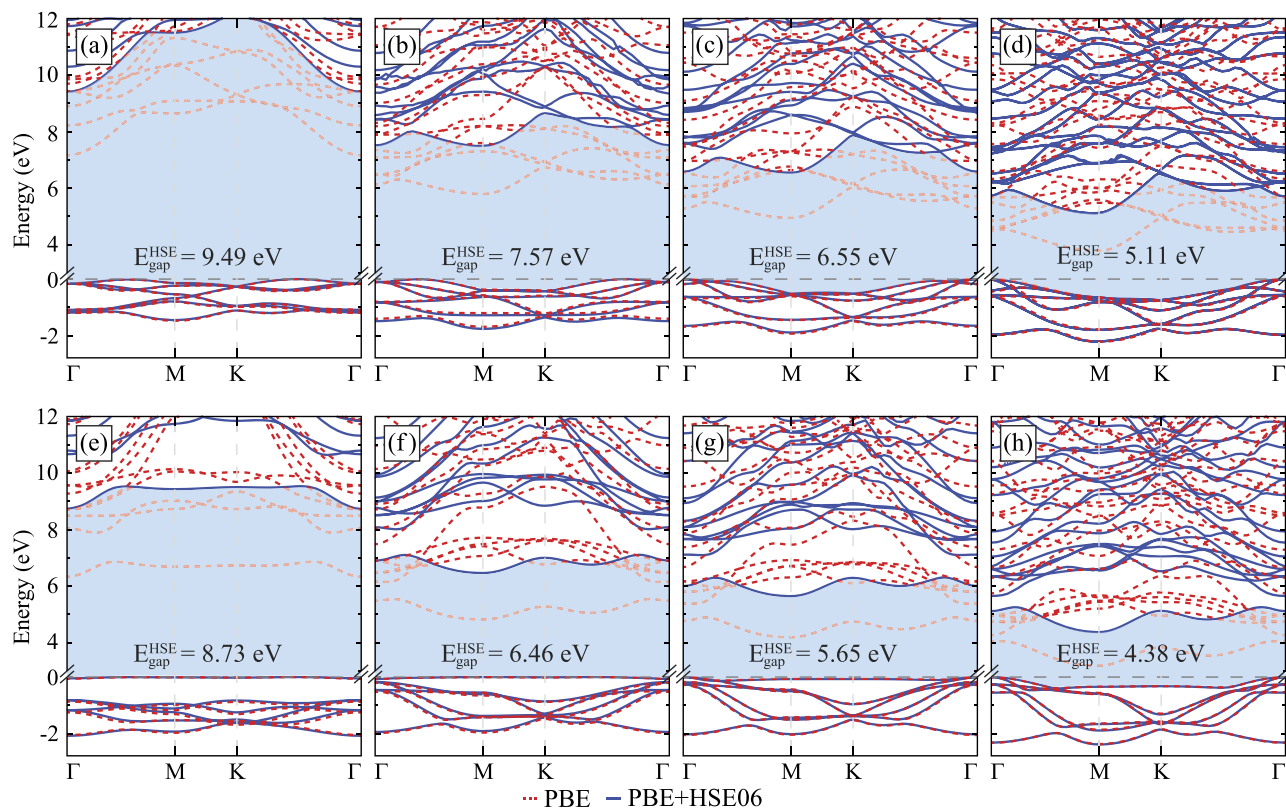


FIG. 4. Electronic band structure of (a) 1T- CaF_2 , (b) 1T- CaCl_2 , (c) 1T- CaBr_2 , (d) 1T- CaI_2 , (e) 1H- CaF_2 , (f) 1H- CaCl_2 , (g) 1H- CaBr_2 , and (h) 1H- CaI_2 .

linear-elastic constants, the elastic strain tensor elements, C_{ij} , are calculated and the corresponding C and ν values, which are isotropic for all directions in the structures, are calculated and the results are listed in Table I. The in-plane stiffness and the Poisson ratio are calculated using the formula

$$C = \frac{(C_{11}C_{22} - C_{12}^2)}{C_{22}}, \quad (1)$$

$$\nu = \frac{C_{12}}{C_{22}}. \quad (2)$$

As listed in Table I, the calculated in-plane stiffness values indicate the ultra-soft nature of the CaX_2 structures in both phases. As compared to the planar single-layers of graphene (330 N/m)^{67,68} and *h*-BN (273 N/m),⁶⁸ the single-layers of both 1T- and 1H- CaX_2 structures are very soft materials. Among the non-planar single-layers such as MoS_2 (122 N/m)^{67,68} and WS_2 (122 N/m),⁶⁸ the Ca-X bonds are weak due to the much smaller in-plane stiffness of the CaX_2 structures. In contrast, the single-layers of CaX_2 have in-plane stiffness that is comparable to those for silicene (54 N/m)⁶⁸ and germanene (34 N/m).⁶⁸ Moreover, the calculated in-plane stiffness values are almost close to each other for the 1T- and 1H-phases of each CaX_2 , indicating similar bonding characteristics in both phases. On the other hand, the Poisson ratios are calculated to be much larger for 1H- CaX_2 structures as compared to their values for 1T-phases. Such relatively large Poisson ratios of 1H- CaX_2 single-layers suggest a more sensitive structural response to external loads, which can be beneficial for nanoelastic applications.

The properties of 1T and 1H phases of CaX_2 single-layers are compared by means of the charge transfer between Ca-X atoms, in-plane stiffness, cohesive energy, and work function, as shown in Fig. 3. The charge donated by a Ca atom in both phases of all single-layers exhibits a decreasing trend as the atomic radius increases [see Fig. 3(a)]. The in-plane stiffness of 1H and 1T phases shows a decreasing trend from F to I structures; however, the relation between 1H and 1T phases for in-plane stiffness changes for CaF_2 arising from slightly smaller charge donation in 1H- CaF_2 . The cohesive energies of the halide structures show a decreasing trend with an increase in the atomic radius, and in all structures, the 1T phase is found to be energetically favorable. A decreasing trend for the work functions of CaX_2 single-layers is shown in accordance with electronegativity of the halogen atoms that is related to atom positions in the Periodic Table. Related to the slightly different charge transfer to the F atom in its 1T and 1H phases, the differences between their work functions are the higher for CaF_2 structures.

B. Electronic properties

The electronic properties of single-layer CaX_2 phases are investigated in terms of their electronic band dispersions, and they are presented in Fig. 4. Bare-GGA and HSE06 approximations reveal that both 1T- or 1H- CaX_2 structures are insulators. The calculated bandgap values are found to be 9.49 eV, 7.57 eV, 6.55 eV, and 5.11 eV for 1T- CaX_2 such that a decreasing trend is found as the halogen atom changes from F to I. A similar trend is found for the single-layers of 1H- CaX_2 such that the bandgap is 8.73 eV for CaF_2 and decreases to 4.38 eV for CaI_2 .

The location of the valence and conduction band edges indicates that all eight single-layer structures of CaX_2 are indirect bandgap insulators. For the single-layers of 1H- CaF_2 and 1H- CaCl_2 , the valence band maximum (VBM) is located in between the M and the K points, while it shifts to the Γ point as the halogen atom changes to Br and I. On the other hand, the conduction band minimum (CBM) is found to reside at the Γ point for 1H- CaF_2 , and it resides at the M point in the other three 1H-phase single-layers. Note that the top valence band is more dispersive in 1H- CaBr_2 and 1H- CaI_2 single-layers. In the case of 1T- CaX_2 single-layers, the CBM resides at the same points as 1H structures. However, for 1T- CaF_2 and 1T- CaCl_2 , the VBM is found to reside in between the K and the Γ points, while it is located at the Γ point for the other two 1T single-layers.

For the modification of the electronic properties of ultra-thin materials, construction of heterostructures is quite important. In a typical vdW heterostructure, the band alignment comparison was shown to be an important method.^{69–73} Three types of band alignments exist in heterojunctions: straddling gap, staggered gap, and broken gap heterojunctions are referred to as type-I, type-II, and type-III, respectively.⁷⁴ Band alignment of CaX_2 in 1T and 1H

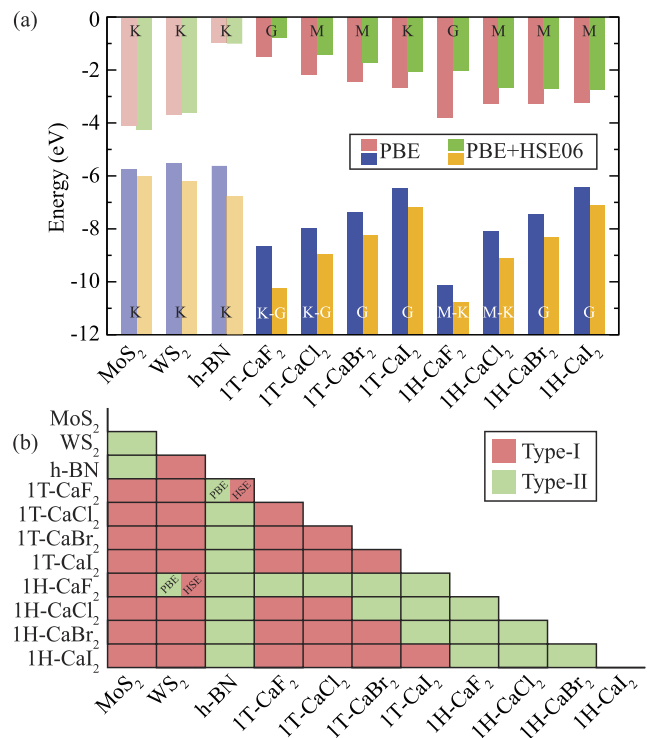


FIG. 5. (a) Comparative band alignment of MoS_2 , WS_2 , *h*-BN, 1T- CaF_2 , 1T- CaCl_2 , 1T- CaBr_2 , 1T- CaI_2 , 1H- CaF_2 , 1H- CaCl_2 , 1H- CaBr_2 , and 1H- CaI_2 where vacuum energies are set to zero. (b) Table for the type of heterojunctions. Blue and red bars represent the valence and conduction bands of GGA results, while orange and green bars represent the valence and conduction bands of the HSE06 approximation. The crystals investigated in this article are displayed with darker color. On each bar, the location of VBM and CBM are also given. Red and green boxes in the table are for type-I and type-II, respectively.

structures along with well-known semiconducting single-layer materials MoS_2 and WS_2 and single-layer insulator h -BN is presented in Fig. 5(a), and the heterojunction types of these crystals are displayed in Fig. 5(b). The results show that all the 1T- and 1H- CaX_2 structures reported in this study form type-I heterojunction with the semiconducting materials such as MoS_2 and WS_2 , while they form type-II heterojunction with h -BN. In addition, the HSE06 approximation is also used to determine the types of band alignments. Calculations reveal that the alignment between $\text{WS}_2/1\text{H-CaF}_2$ and h -BN/1T- CaF_2 structures switches to type-I. The rest of the band alignments remain the same alignment type.

IV. CONCLUSIONS

In this study, the structural, vibrational, and electronic properties of 1H- and 1T-phases of single-layer CaX_2 ($X = \text{F}, \text{Cl}, \text{Br}$, or I) structures were investigated. Our results revealed that the 1T-phase of CaX_2 is energetically favorable for all halogen atoms and both 1T- and 1H-phases were found to be dynamically stable in terms of their phonon band dispersions. Either in the 1H- or in the 1T-phase, significant phonon softening was found as the atomic radius increases from the F to I structure. In addition, 1T- CaX_2 exhibit one doubly degenerate in-plane Raman active mode and one non-degenerate out-of-plane Raman active mode, while for 1H structures, there are three Raman active modes (two doubly degenerate and one non-degenerate) arising from the different symmetries in the structures. Moreover, the electronic band dispersions of single-layer CaX_2 structures indicated the indirect bandgap insulating nature of all single-layers with a decrease in bandgaps from F to I crystals. Furthermore, the calculated linear elastic constants, in-plane stiffness, and Poisson ratio showed the ultra-soft nature of CaX_2 single-layers, which is quite important for their nanoelastic applications. Overall, our study revealed that with their dynamically stable 1T- and 1H-phases, single-layers of CaX_2 crystals can be alternative insulators to the well-known single-layer h -BN.

ACKNOWLEDGMENTS

Computational resources were provided by TUBITAK ULAK-BIM, High Performance and Grid Computing Center (TR-Grid e-Infrastructure). H.S. acknowledges financial support from the TUBITAK under Project No. 117F095. H.S. acknowledges support from the Turkish Academy of Sciences under the GEBIP program. M.Y. was supported by a postdoctoral fellowship from the Flemish Science Foundation (FWO-VI).

REFERENCES

¹K. S. Novoselov, A. K. Geim, S. V. Morozov, D. Jiang, Y. Zhang, S. V. Dubonos, I. V. Grigorieva, and A. A. Firsov, "Electric field effect in atomically thin carbon films," *Science* **306**, 666–669 (2004).
²A. K. Geim and K. S. Novoselov, *Nanoscience and Technology: A Collection of Reviews from Nature Journals* (World Scientific, 2010), pp. 11–19.
³Q. H. Wang, K. Kalantar-Zadeh, A. Kis, J. N. Coleman, and M. S. Strano, "Electronics and optoelectronics of two-dimensional transition metal dichalcogenides," *Nat. Nanotechnol.* **7**, 699 (2012).

⁴M. Chhowalla, H. S. Shin, G. Eda, L.-J. Li, K. P. Loh, and H. Zhang, "The chemistry of two-dimensional layered transition metal dichalcogenide nanosheets," *Nat. Chem.* **5**, 263 (2013).
⁵A. Ramasubramanian, "Large excitonic effects in monolayers of molybdenum and tungsten dichalcogenides," *Phys. Rev. B* **86**, 115409 (2012).
⁶K. F. Mak, C. Lee, J. Hone, J. Shan, and T. F. Heinz, "Atomically thin MoS_2 : A new direct-gap semiconductor," *Phys. Rev. Lett.* **105**, 136805 (2010).
⁷B. Radisavljevic, A. Radenovic, J. Brivio, V. Giacometti, and A. Kis, "Single-layer MoS_2 transistors," *Nat. Nanotechnol.* **6**, 147 (2011).
⁸S. Tongay, J. Zhou, C. Ataca, K. Lo, T. S. Matthews, J. Li, J. C. Grossman, and J. Wu, "Thermally driven crossover from indirect toward direct bandgap in 2D semiconductors: MoSe_2 versus MoS_2 ," *Nano Lett.* **12**, 5576–5580 (2012).
⁹T. Georgiou, R. Jalil, B. D. Belle, L. Britnell, R. V. Gorbachev, S. V. Morozov, Y.-J. Kim, A. Gholinia, S. J. Haigh, O. Makarovsky, L. Eaves, L. A. Ponomarenko, A. K. Geim, K. S. Novoselov, and A. Mishchenko, "Vertical field-effect transistor based on graphene- WS_2 heterostructures for flexible and transparent electronics," *Nat. Nanotechnol.* **8**, 100 (2013).
¹⁰H. Fang, S. Chuang, T. C. Chang, K. Takei, T. Takahashi, and A. Javey, "High-performance single layered WSe_2 p-FETs with chemically doped contacts," *Nano Lett.* **12**, 3788–3792 (2012).
¹¹J. S. Ross, P. Klement, A. M. Jones, N. J. Ghimire, J. Yan, D. G. Mandrus, T. Taniguchi, K. Watanabe, K. Kitamura, W. Yao, D. H. Cobden, and X. Xu, "Electrically tunable excitonic light-emitting diodes based on monolayer WSe_2 p-n junctions," *Nat. Nanotechnol.* **9**, 268 (2014).
¹²S. Tongay *et al.*, "Monolayer behaviour in bulk ReS_2 due to electronic and vibrational decoupling," *Nat. Commun.* **5**, 3252 (2014).
¹³A. Molle, J. Goldberger, M. Houssa, Y. Xu, S.-C. Zhang, and D. Akinwande, "Buckled two-dimensional Xene sheets," *Nat. Mater.* **16**, 163–169 (2017).
¹⁴H. Şahin, S. Cahangirov, M. Topsakal, E. Bekaroglu, E. Akturk, R. T. Senger, and S. Ciraci, "Monolayer honeycomb structures of group-IV elements and III-V binary compounds: First-principles calculations," *Phys. Rev. B* **80**, 155453 (2009).
¹⁵L. Matthes, O. Pulci, and F. Bechstedt, "Optical properties of two-dimensional honeycomb crystals graphene, silicene, germanene, and tinene from first principles," *New J. Phys.* **16**, 105007 (2014).
¹⁶P. Vogt, P. De Padova, C. Quaresima, J. Avila, E. Frantzeskakis, M. C. Asensio, A. Resta, B. Ealet, and G. Le Lay, "Silicene: Compelling experimental evidence for graphenelike two-dimensional silicon," *Phys. Rev. Lett.* **108**, 155501 (2012).
¹⁷M. E. Dávila, L. Xian, S. Cahangirov, A. Rubio, and G. Le Lay, "Germanene: A novel two-dimensional germanium allotrope akin to graphene and silicene," *New J. Phys.* **16**, 095002 (2014).
¹⁸F.-f. Zhu, W.-j. Chen, Y. Xu, C.-l. Gao, D.-d. Guan, C.-h. Liu, D. Qian, S.-C. Zhang, and J.-f. Jia, "Epitaxial growth of two-dimensional stanene," *Nat. Mater.* **14**, 1020 (2015).
¹⁹B. Cai, S. Zhang, Z. Hu, Y. Hu, Y. Zou, and H. Zeng, "Tinene: A two-dimensional Dirac material with a 72 meV band gap," *Phys. Chem. Chem. Phys.* **17**, 12634–12638 (2015).
²⁰X.-L. Yu, L. Huang, and J. Wu, "From a normal insulator to a topological insulator in plumbene," *Phys. Rev. B* **95**, 125113 (2017).
²¹C. Gong, L. Li, Z. Li, H. Ji, A. Stern, Y. Xia, T. Cao, W. Bao, C. Wang, Y. Wang, Z. Q. Qiu, R. J. Cava, S. G. Louie, J. Xia, and X. Zhang, "Discovery of intrinsic ferromagnetism in two-dimensional van der Waals crystals," *Nature* **546**, 265 (2017).
²²B. Huang, G. Clark, E. Navarro-Moratalla, D. R. Klein, R. Cheng, K. L. Seyler, D. Zhong, E. Schmidgall, M. A. McGuire, D. H. Cobden, W. Yao, D. Xiao, P. Jarillo-Herrero, and X. Xu, "Layer-dependent ferromagnetism in a van der Waals crystal down to the monolayer limit," *Nature* **546**, 270 (2017).
²³K. L. Seyler, D. Zhong, D. R. Klein, S. Gao, X. Zhang, B. Huang, E. Navarro-Moratalla, L. Yang, D. H. Cobden, M. A. McGuire, W. Yao, D. Xiao, P. Jarillo-Herrero, and X. Xu, "Ligand-field helical luminescence in a 2D ferromagnetic insulator," *Nat. Phys.* **14**, 277 (2018).
²⁴W. Xing, Y. Chen, P. M. Odenthal, X. Zhang, W. Yuan, T. Su, Q. Song, T. Wang, J. Zhong, S. Jia, X. C. Xie, Y. Li, and W. Han, "Electric field effect

- in multilayer $\text{Cr}_2\text{Ge}_2\text{Te}_6$: A ferromagnetic 2D material," *2D Mater.* **4**, 024009 (2017).
- ²⁵T. Kong, K. Stolze, E. I. Timmons, J. Tao, D. Ni, S. Guo, Z. Yang, R. Prozorov, and R. J. Cava, "VI₃—a new layered ferromagnetic semiconductor," *Adv. Mater.* **31**, 1808074 (2019).
- ²⁶M. Baskurt, I. Eren, M. Yagmurcukardes, and H. Sahin, "Vanadium dopant- and strain-dependent magnetic properties of single-layer VI₃," *Appl. Surf. Sci.* **508**, 144937 (2020).
- ²⁷L. H. Li and Y. Chen, "Atomically thin boron nitride: Unique properties and applications," *Adv. Funct. Mater.* **26**, 2594–2608 (2016).
- ²⁸K. Watanabe, T. Taniguchi, and H. Kanda, "Direct-bandgap properties and evidence for ultraviolet lasing of hexagonal boron nitride single crystal," *Nat. Mater.* **3**, 404 (2004).
- ²⁹H. Jeong, S. Bang, H. M. Oh, H. J. Jeong, S.-J. An, G. H. Han, H. Kim, K. K. Kim, J. C. Park, Y. H. Lee, G. Lerondel, and M. S. Jeong, "Semiconductor-insulator-semiconductor diode consisting of monolayer MoS₂, h-BN, and GaN heterostructure," *ACS Nano* **9**, 10032–10038 (2015).
- ³⁰M. P. Levendorf, C.-J. Kim, L. Brown, P. Y. Huang, R. W. Havener, D. A. Muller, and J. Park, "Graphene and boron nitride lateral heterostructures for atomically thin circuitry," *Nature* **488**, 627 (2012).
- ³¹S. Ahn, G. Kim, P. K. Nayak, S. I. Yoon, H. Lim, H.-J. Shin, and H. S. Shin, "Prevention of transition metal dichalcogenide photodegradation by encapsulation with h-BN layers," *ACS Nano* **10**, 8973–8979 (2016).
- ³²J. G. Speight, *Environmental Organic Chemistry for Engineers* (Butterworth-Heinemann, 2016).
- ³³L. Sun and L. C. Chow, "Preparation and properties of nano-sized calcium fluoride for dental applications," *Dent. Mater.* **24**, 111–116 (2008).
- ³⁴H. H. K. Xu, J. L. Moreau, L. Sun, and L. C. Chow, "Strength and fluoride release characteristics of a calcium fluoride based dental nanocomposite," *Biomaterials* **29**, 4261–4267 (2008).
- ³⁵D. S. Brauer, N. Karpukhina, R. V. Law, and R. G. Hill, "Structure of fluoride-containing bioactive glasses," *J. Mater. Chem.* **19**, 5629–5636 (2009).
- ³⁶L. Cheng, M. D. Weir, H. H. K. Xu, A. M. Kraigsley, N. J. Lin, S. Lin-Gibson, and X. Zhou, "Antibacterial and physical properties of calcium-phosphate and calcium-fluoride nanocomposites with chlorhexidine," *Dent. Mater.* **28**, 573–583 (2012).
- ³⁷A. Al-Noaman, S. C. F. Rawlinson, and R. G. Hill, "The influence of CaF₂ content on the physical properties and apatite formation of bioactive glass coatings for dental implants," *J. Non-Cryst. Solids* **358**, 1850–1858 (2012).
- ³⁸A. Lucca, M. Jacquemet, F. Druon, F. Balembois, P. Georges, P. Camy, J. L. Doualan, and R. Moncorgé, "High-power tunable diode-pumped Yb³⁺: CaF₂ laser," *Opt. Lett.* **29**, 1879–1881 (2004).
- ³⁹A. Lucca, G. Debourg, M. Jacquemet, F. Druon, F. Balembois, P. Georges, P. Camy, J. L. Doualan, and R. Moncorgé, "High-power diode-pumped Yb³⁺: CaF₂ femtosecond laser," *Opt. Lett.* **29**, 2767–2769 (2004).
- ⁴⁰M. Siebold, S. Bock, U. Schramm, B. Xu, J. L. Doualan, P. Camy, and R. Moncorgé, "CaF₂—a new old laser crystal," *Appl. Phys. B* **97**, 327–338 (2009).
- ⁴¹P. Aubry, A. Bensalah, P. Gredin, G. Patriarche, D. Vivien, and M. Mortier, "Synthesis and optical characterizations of Yb-doped CaF₂ ceramics," *Opt. Mater.* **31**, 750–753 (2009).
- ⁴²M. S. Akchurin, T. T. Basiev, A. A. Demidenko, M. E. Doroshenko, P. P. Fedorov, E. A. Garibin, P. E. Gusev, S. V. Kuznetsov, M. A. Krutov, I. A. Mironov, V. V. Osiko, and P. A. Popov, "CaF₂: Yb laser ceramics," *Opt. Mater.* **35**, 444–450 (2013).
- ⁴³M. Baskurt, J. Kang, and H. Sahin, "Octahedrally coordinated single layer CaF₂: Robust insulating behaviour," *Phys. Chem. Chem. Phys.* **22**, 2949–2954 (2020).
- ⁴⁴R. Robinson and R. Stokes, *Electrolyte Solutions*, 2nd rev. ed., Dover Books on Chemistry Series (Dover Publications, 2012).
- ⁴⁵X. M. Wu, Y. S. Yu, C. Y. Zhang, G. X. Wang, and B. Feng, "Identifying the CO₂ capture performance of CaCl₂-supported amine adsorbent by the improved field synergy theory," *Ind. Eng. Chem. Res.* **53**, 10225–10237 (2014).
- ⁴⁶X. M. Wu, D. L. Mu, Y. S. Yu, and Z. X. Zhang, "String to characterize the field synergy during CO₂ capture by CaCl₂-supported MEA adsorbent," *J. Phys. Chem. C* **119**, 473–485 (2014).
- ⁴⁷L. Kou, T. Yang, Y. Luo, X. Liu, L. Huang, and E. Codling, "Pre-harvest calcium application increases biomass and delays senescence of broccoli microgreens," *Postharvest Biol. Technol.* **87**, 70–78 (2014).
- ⁴⁸J. Sun, L. Kou, P. Geng, H. Huang, T. Yang, Y. Luo, and P. Chen, "Metabolomic assessment reveals an elevated level of glucosinolate content in CaCl₂ treated broccoli microgreens," *J. Agric. Food Chem.* **63**, 1863–1868 (2015).
- ⁴⁹L. Wang, L. Ma, H. Xi, W. Duan, J. Wang, and S. Li, "Individual and combined effects of CaCl₂ and UV-C on the biosynthesis of resveratrol in grape leaves and berry skins," *J. Agric. Food Chem.* **61**, 7135–7141 (2013).
- ⁵⁰C. Y. Liu and K.-i. Aika, "Ammonia absorption into alkaline earth metal halide mixtures as an ammonia storage material," *Ind. Eng. Chem. Res.* **43**, 7484–7491 (2004).
- ⁵¹C. Y. Liu and K.-i. Aika, "Effect of the Cl/Br molar ratio of a CaCl₂-CaBr₂ mixture used as an ammonia storage material," *Ind. Eng. Chem. Res.* **43**, 6994–7000 (2004).
- ⁵²S. Al-Asheh and F. Banat, "Isobaric vapor-liquid equilibrium of acetone+ methanol system in the presence of calcium bromide," *J. Chem. Eng. Data* **50**, 1789–1793 (2005).
- ⁵³L. Kumar, T. Mahajan, V. Sharma, and D. D. Agarwal, "Environmentally-benign and rapid bromination of industrially-important aromatics using an aqueous CaBr₂-Br₂ system as an instant and renewable brominating reagent," *Ind. Eng. Chem. Res.* **50**, 705–712 (2010).
- ⁵⁴N. Kanai, H. Nakayama, N. Tada, and A. Itoh, "Tandem oxidation/rearrangement of β -ketoesters to tartronic esters with molecular oxygen catalyzed by calcium iodide under visible light irradiation with fluorescent lamp," *Org. Lett.* **12**, 1948–1951 (2010).
- ⁵⁵L. Longwitz, J. Steinbauer, A. Spannenberg, and T. Werner, "Calcium-based catalytic system for the synthesis of bio-derived cyclic carbonates under mild conditions," *ACS Catal.* **8**, 665–672 (2017).
- ⁵⁶Y. Hu, J. Steinbauer, V. Stefanow, A. Spannenberg, and T. Werner, "Polyethers as complexing agents in calcium catalyzed cyclic carbonate synthesis," *ACS Sustainable Chem. Eng.* **7**, 13257 (2019).
- ⁵⁷F. Lu, W. Wang, X. Luo, X. Xie, Y. Cheng, H. Dong, H. Liu, and W.-H. Wang, "A class of monolayer metal halogenides MX₂: Electronic structures and band alignments," *Appl. Phys. Lett.* **108**, 132104 (2016).
- ⁵⁸G. Bhattacharyya, P. Garg, P. Bhauriyal, and B. Pathak, "Density functional theory study of defect induced ferromagnetism and half-metallicity in CaI₂ based monolayer for spintronics applications," *ACS Appl. Nano Mater.* **2**, 6152–6161 (2019).
- ⁵⁹G. Kresse and J. Hafner, "Ab initio molecular dynamics for liquid metals," *Phys. Rev. B* **47**, 558 (1993).
- ⁶⁰G. Kresse and J. Furthmüller, "Efficient iterative schemes for *ab initio* total-energy calculations using a plane-wave basis set," *Phys. Rev. B* **54**, 11169 (1996).
- ⁶¹P. E. Blöchl, "Projector augmented-wave method," *Phys. Rev. B* **50**, 17953–17979 (1994).
- ⁶²J. P. Perdew, K. Burke, and M. Ernzerhof, "Generalized gradient approximation made simple," *Phys. Rev. Lett.* **77**, 3865–3868 (1996).
- ⁶³S. Grimme, "Semiempirical GGA-type density functional constructed with a long-range dispersion correction," *J. Comput. Chem.* **27**, 1787–1799 (2006).
- ⁶⁴J. Heyd, G. E. Scuseria, and M. Ernzerhof, "Hybrid functionals based on a screened Coulomb potential," *J. Chem. Phys.* **118**, 8207–8215 (2003).
- ⁶⁵G. Henkelman, A. Arnaldsson, and H. Jónsson, "A fast and robust algorithm for Bader decomposition of charge density," *Comput. Mater. Sci.* **36**, 354–360 (2006).
- ⁶⁶D. Alfè, "A program to calculate phonons using the small displacement method," *Comput. Phys. Commun.* **180**, 2622–2633 (2009).
- ⁶⁷M. Yagmurcukardes, R. Senger, F. Peeters, and H. Sahin, "Mechanical properties of monolayer GaS and GaSe crystals," *Phys. Rev. B* **94**, 245407 (2016).
- ⁶⁸M. Yagmurcukardes, C. Bacaksiz, E. Unsal, B. Akbali, R. Senger, and H. Sahin, "Strain mapping in single-layer two-dimensional crystals via Raman activity," *Phys. Rev. B* **97**, 115427 (2018).
- ⁶⁹D. O. Scanlon, C. W. Dunnill, J. Buckeridge, S. A. Shevlin, A. J. Logsdail, S. M. Woodley, C. R. A. Catlow, M. J. Powell, R. G. Palgrave, I. P. Parkin, G. W.

Watson, T. W. Keal, P. Sherwood, A. Walsh, and A. A. Sokol, "Band Alignment of rutile and anatase TiO_2 ," *Nat. Mater.* **12**, 798 (2013).

⁷⁰V. O. Özcelik, J. G. Azadani, C. Yang, S. J. Koester, and T. Low, "Band Alignment of two-dimensional semiconductors for designing heterostructures with momentum space matching," *Phys. Rev. B* **94**, 035125 (2016).

⁷¹M. Yagmurcukardes, E. Torun, R. T. Senger, F. M. Peeters, and H. Sahin, " $\text{Mg}(\text{OH})_2$ - WS_2 van der Waals heterobilayer: Electric field tunable band-gap crossover," *Phys. Rev. B* **94**, 195403 (2016).

⁷²Z. Kahraman, A. Kandemir, M. Yagmurcukardes, and H. Sahin, "Single-layer Janus-type platinum dichalcogenides and their heterostructures," *J. Phys. Chem. C* **123**, 4549–4557 (2019).

⁷³M. Yagmurcukardes, S. Ozen, F. Iyikanat, F. Peeters, and H. Sahin, "Raman fingerprint of stacking order in HfS_2 - $\text{Ca}(\text{OH})_2$ heterobilayer," *Phys. Rev. B* **99**, 205405 (2019).

⁷⁴T. Ihn, *Semiconductor Nanostructures: Quantum States and Electronic Transport* (Oxford University Press, 2010).